12.2 bit/s/Hz C-band Transmission with High-Gain Low-Complexity 24-Dimensional Geometric Shaping

12.2 bit/s/Hz C-band Transmission with High-Gain Low-Complexity 24-Dimensional Geometric Shaping

Zonglong He, Shen Li, Ekaterina Deriushkina, Peter Andrekson, *Fellow, IEEE, Fellow, Optica*, Erik Agrell, *Fellow, IEEE*, Magnus Karlsson, *Fellow, IEEE, Fellow, Optica*, and Jochen Schröder, *Member, IEEE, Senior Member, Optica*

***Abstract*—Multidimensional (MD) modulation formats enable a larger minimum Euclidean distance than conventional two-dimensional formats. As a structured geometric shaping method, MD Voronoi constellations (VCs) avoid the use of look-up tables and can be implemented with low-complexity encoding and decoding algorithms, outperforming quadrature amplitude modulation (QAM) formats in terms of mutual information. However, it is challenging to maintain the shaping gain in a practical system requiring bit-mapping and forward error correction (FEC) coding. By using a hybrid labeling and multilevel coding scheme integrated with soft-decision FEC coding, MD VCs can achieve high shaping gain compared to QAM formats after soft-decision (SD) decoding. In practical systems, transceiver impairments significantly degrade the system performance, especially for high-cardinality constellations. To investigate of performance of high spectral-efficiency (SE) MD VCs, we employ a 24-dimensional (24D) VC with uncoded SE of 8 bit/symbol/dimension-pair to a spectral superchannel spanning the full C-band. Specifically, the 24D VC with a record constellation size of 7.9×10^{28} is applied to dual-polarization coherent transmission over six time slots. The superchannel is composed of 5.0 Gbaud channels spaced at 5.2 GHz, resulting in an overall spectral efficiency of 12.2 bit/s/Hz and a net throughput of 54.2 Tb/s over the entire C-band after 40 km single-mode fiber. It is the first experimental demonstration of a high-SE MD format providing a significant shaping gain after SD decoding.**

***Index Terms*—Coherent communications, multidimensional formats, Voronoi constellation, lattice, geometric shaping, superchannel, spectral efficiency, wideband transmission, capacity**

I. Introduction

HIGH spectral efficiency (SE) and throughput are the key performance metrics for modern dense wavelength division multiplexing transmission systems, requiring advanced modulation formats such as high-order quadrature amplitude modulation (QAM) and forward error correction (FEC). To facilitate the large-symbol-rate and high-spectral-efficiency applications, pre-distortion is commonly applied to overcome the bandwidth limitations of the electrical components and the nonlinear distortion induced by the IQ modulators/RF amplifiers [1]. Importantly, advanced digital signal processing (DSP) is required to compensate for other impairments such as chromatic dispersion, polarization mode dispersion, laser frequency offset/phase noise, and even fiber nonlinearity [2]. Recently, modern 800G high-speed transponders have become commercially available by employing 96-Gbaud 64QAM signals [3]–[5]. Amongst various recent high-SE broadband experiments [6]–[13], the highest C-band bit rate of 72.64 Tb/s and SE of 12.29 bit/s/Hz was demonstrated using 43×130 GBaud dual-polarization (DP) 256QAM [6] with probabilistic shaping (PS). In [12], 34×130 Gbaud DP-PS-400QAM/256QAM was transmitted over a 95.5 km single-mode fiber (SMF), achieving SEs of 10.92/11.08 bit/s/Hz, respectively.

In contrast to conventional QAM formats, constellation shaping changes either the geometry location or probability distribution of the constellation to approximate the Gaussian distribution [14], referred to as geometric shaping (GS) and PS respectively. While PS enables exceptional shaping gain and rate adaptivity, it requires a distribution matcher (DM) [15] which significantly increases the implementation complexity and the resulting additional latency might be undesired for some low-latency applications (e.g., remote meetings, online gaming, and trading). Optimized 2-dimensional (2D) GS constellations have been widely studied and shown to achieve larger shaping gain for a higher cardinality [16]. However, the increased implementation complexity and aforementioned transmitter impairments inhibit the usage of high-order formats and result in limited gain. The irregular constellation shape of GS can lead to incompatibility with Gray-mapping, requiring special labeling and demapping methods (e.g., end-to-end learning [17]).

Given the same average symbol energy, advanced multi-dimensional (MD) modulation formats are designed to have a larger minimum Euclidean distance (MED) than conventional 2D QAM formats and can provide a higher degree of freedom to alleviate fiber nonlinearity [18]–[20]. Generally, MD formats can be created by set-partitioning [21], spherical lattice cuts [22], polarization switching [23], or using biorthogonal modulation [24], [25]. A class of modulation

This work was supported by the Knut and Alice Wallenberg Foundation under grant No. 2018-0090, and the Swedish Research Council (VR) under grant No. 2019-04078 and 2021-03709. (*Corresponding author: Zonglong He*)

Z. He, E. Deriushkina, P. Andrekson, M. Karlsson, and J. Schröder are with the Photonics Laboratory, Fibre Optic Communication Research Centre (FORCE), Department of Microtechnology and Nanoscience, Chalmers University of Technology, Gothenburg 41296, Sweden (e-mail: zonglong@chalmers.se; ekader@chalmers.se; peter.andrekson@chalmers.se; magnus.karlsson@chalmers.se; jochen.schroeder@chalmers.se).

E. Agrell is with the Department of Electrical Engineering, Chalmers University of Technology, Gothenburg 41296, Sweden (email: agrell@chalmers.se)

S. Li was with the Department of Electrical Engineering, Chalmers University of Technology, Gothenburg 41296, Sweden and is now with Centre of Optics, Photonics and Lasers (COPL), Department of Electrical and Computer Engineering, Université Laval, Québec, Canada (email: shen.li.1@ulaval.ca)

format of particular interest are MD Voronoi constellations (VCs) [26], [27]. MD VCs have demonstrated better bit error rate (BER) performance than Gray-labeled QAM in uncoded systems [28], [29] below the hard-decision (HD) FEC threshold, and as a structured geometric shaping method, they have low-complexity encoding [26] and decoding algorithms [30], [31] avoiding the need for look-up tables to store all MD symbols. However, most of the MD formats provide shaping gain over QAM at pre-FEC BERs between 10^{-3} and 10^{-2} [22], [28], [29], [32]. With separate modulation and FEC coding, the above-mentioned MD formats perform worse than conventional QAM formats at a pre-FEC BER threshold of 2.7×10^{-2} in metro and long-haul transmission system.

In terms of mutual information (MI), VCs showed high gains over QAM [33], [34], which indicates a potential for high-performance coded modulation. Recently, a multilevel coding (MLC) scheme with soft-decision (SD) FEC codes was designed for VCs for the first time [35], preserving the high shaping gains of very large VCs after low-complexity SD decoding. In contrast to bit-interleaved coded modulation (BICM), which has been used in almost all high-SE transmission experiments, the MLC scheme is optimal as the underlying design criterion is the MI following the chain rule. In contrast, the upper bound of the achievable information rate of BICM is the generalized mutual information (GMI), leading to an information loss when there is a gap between the MI and GMI of the constellation. Compared to PS, which requires a large-block DM and therefore is computationally expensive, the proposed MD VCs in [35] can achieve comparable gain with lower complexity.

In this paper, we use the MLC scheme proposed in [35] as SD-FEC and experimentally present C-band transmission of 854×5.0 Gbaud 24-dimensional (24D) VC with a record constellation size of 7.9×10^{28}. The 24D VC is implemented over quadratures, both polarizations, and six time slots. Assuming a MLC SD-FEC OH of 14.29% and an outer HD-FEC OH of 6.25%, the results show that the proposed 24D VC achieves 1.1 dB OSNR shaping gain over 256-QAM tested at three wavelengths 1531.45 nm, 1546.63 nm, and 1559.11 nm, and maintains a high SE of 12.2 bit/s/Hz and a net throughput of 54.2 Tb/s after 40 km SMF transmission. To the best of our knowledge, this is the first experimental demonstration of a high-SE (>12 bit/s/Hz) MD modulation format with a significant shaping gain after SD-FEC decoding.

The remainder of the paper is organized as follows. In Section II, the MD VCs are introduced. In Section III, we briefly describe the MLC scheme used for VCs. In Section IV, the simulation results including a comparison of various signal formats (i.e., VCs and QAM) and the optimization of SD-FEC overhead (OH) are shown for the multidimensional additive white Gaussian noise (AWGN) channel. The experimental setup and results for C-band transmission are demonstrated in Section V and VI, respectively. Finally, we present the conclusion in Section VII.

II. Voronoi Constellations

VCs are lattice-based zero-mean MD modulation formats [36], [37], which provide structured geometric shaping. A

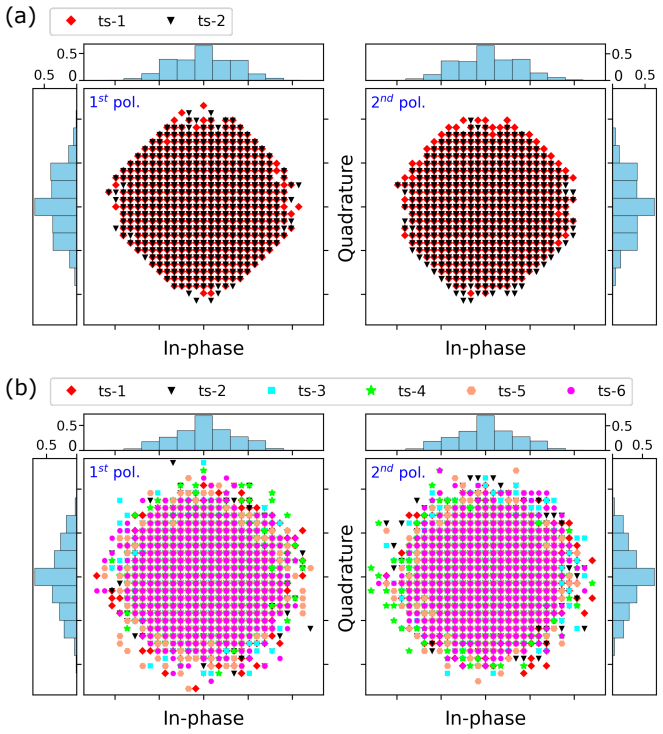

Fig. 1. 1D and 2D (i.e., in-phase and quadrature) projections of the (a) 8D, (b) 24D Voronoi constellation, including various time slots (ts) plotted with different markers and colors for each polarization (pol.). Specifically, the 1D projection shows the probability distribution of the MD Voronoi constellation at each dimension.

key benefit over optimized GS constellations is that VCs need no look-up tables for storing the constellation points and no full search for demodulation. They can hence be scaled up to enormous constellation sizes without complexity problems. A VC consists of a shaping lattice and a coding lattice, which determines the boundary and packing structure of the constellations, respectively. It is important to select a proper shaping lattice to generate a Gaussian-shaped signal and achieve a high shaping gain with fast encoding/decoding (mapping between integers and constellation coordinates) algorithms. Among the commonly used lattices having fast encoding/decoding algorithms, high-dimensional shaping lattices with higher spectral efficiencies potentially provide large shaping gains [33, Fig. 2]. The choice of the coding lattice affects the decoding complexity, labeling rule design, and the analysis of many important metrics of a communication system. A cubic coding lattice with zero coding gain was chosen in [33], [35], primarily because the cubic coding lattice has a small kissing number, making the joint design of effective bit labeling rules and FEC decoding easier. Its simple structure also makes the evaluation/approximation of MI, GMI, and log-likelihood ratios (LLRs) in SD decoding feasible for such huge constellations. Moreover, the cubic coding lattice has a simpler decoding algorithm than any other coding lattice and doubles the granularity of the uncoded spectral efficiency using a "scaled" version of the shaping lattice. The absence of coding gain with a cubic coding lattice is compensated by FEC codes, while the shaping gain is fully provided by the shaping lattice being used.

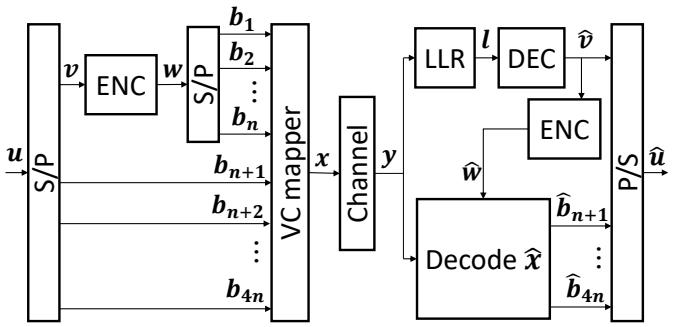

Fig. 2. The SD MLC structure for the 24-dimensional Voronoi constellation, where n is the number of encoding bits and $4n$ is the number of total bits. S: serial, P: parallel, ENC: LDPC encoder, DEC: LDPC decoder; log-likelihood ratio: LLR.

In this paper, the 8-dimensional (8D) and 24-dimensional (24D) VCs denoted by E_8^{32} and Λ_{24}^{96} in [35, Table III], both with an uncoded SE of 8 bit/2D-symbol, are considered and compared with 256-QAM. The two VCs have $2^{32} = 4.3 \times 10^9$ and $2^{96} = 7.9 \times 10^{28}$ constellation points and use the Gosset and Leech lattices for shaping, respectively. Ideally, zero-mean VCs would be generated. For high-SE VCs, a small non-zero mean exists because it is challenging to fully optimize the large-cardinality constellations. However, this small mean has been proven to have negligible influence on VC performance [36, Fig. 3]. Fig. 1 shows the 1-dimensional (1D) and 2D projections of the 8D/24D VC for each polarization. We align most of the symbols from different time-slot dimensions to the same point to reduce the impairments from limited hardware resolution (e.g., the effective number of bit) and facilitate the transmitter nonlinearity mitigation. The number of unique 2D points in each polarization is around 460 for the 8D VC and 540 for the 24D VC. Many 2D points are located in the low-energy regime, thereby approximating a 1D/2D Gaussian probability distribution, which increases the shaping gain. The 1D probability distribution of the 24D VC resembles the Gaussian curve better than the 8D VC, indicating larger achievable shaping gains for higher-dimensional VCs.

III. Multilevel coding for VCs

The conclusion that a MLC scheme, instead of a BICM scheme, is more suitable for VCs, was drawn in [34] where the MI and GMI performance of VCs were compared for nonlinear fiber channels. The results in [34] show that VCs can achieve high MI gains over QAM but limited GMI gains under limited spectral efficiency and SNR. As the GMI assumes a capacity-achieving FEC code, perfect interleaving, and independent labeling of the constellation, it upper-bounds the performance of a BICM scheme, whereas the performance of a CM scheme with multilevel or nonbinary FEC codes is upper-bounded by the MI [38]. Thus, a joint design of an MLC scheme and a "hybrid labeling" was proposed in [35] for VCs to realize the high shaping gains it provides over QAM.

In this paper, following [35, Sec. IV-C], a concatenated CM scheme with an inner SD MLC scheme and an assumed outer binary HD staircase code is applied to the considered VCs. Specifically, the SD MLC scheme is illustrated in Fig. 2. The information bits $\boldsymbol{u}$ are partitioned into $3n$ uncoded bit streams $\boldsymbol{b}_{n+1}, \ldots, \boldsymbol{b}_{4n}$ and one stream $\boldsymbol{v}$ for coding the first n bits, where n is the number of dimensions of the VC having 4 bit/symbol/dimension uncoded SE. Then $\boldsymbol{v}$ is encoded by a binary low-density parity check (LDPC) code with a codeword length of 64800. The encoded bits $\boldsymbol{w}$ are partitioned into n bit streams $\boldsymbol{b}_1, \ldots, \boldsymbol{b}_n$. Finally, the $4n$ bit streams are mapped to n-dimensional (nD) VC symbols $\boldsymbol{x}$ by applying [35, Alg. 3] with $q = p_1 = p = 1$ and then [33, Alg. 1]. The decoding process works as follows. Given noisy nD symbols $\boldsymbol{y}$, the LDPC decoder first decodes $\hat{\boldsymbol{v}}$ based on the LLRs $\boldsymbol{l}$ calculated using [35, Eq. 43–44] with parameters $p_0 = 0, i = p_1 = R^2 = 1, e = 1, \ldots, n$, and $j = 1, \ldots, 64800/n$. Then $\hat{\boldsymbol{v}}$ is encoded into $\hat{\boldsymbol{w}}$, indicating to which lattice subset the estimated VC symbol $\hat{\boldsymbol{x}}$ belongs. By performing a simple closest lattice point algorithm in the underlying subset according to [35, Eq. 37] with $p = 1, \hat{\boldsymbol{c}} = \hat{\boldsymbol{w}}$, and $j = 1, \ldots, 64800/n$, $\hat{\boldsymbol{x}}$ is obtained before demapping it into bits $\hat{\boldsymbol{b}}_{n+1}, \ldots, \hat{\boldsymbol{b}}_{4n}$ using [35, Alg. 4] with $q = p_1 = p = 1$. More details about the hybrid labeling and decoding can be found in [35].

Importantly, the applied MLC scheme, together with the hybrid labeling, partitions the VC into 2^n subsets, doubling the MED within each subset. Therefore, the first n bits of the VC are protected by the LDPC code and the remaining $3n$ bits can stay uncoded due to sufficiently large intra-set MED. The LLR computation involves only a small number of VC points and finding the bit labels of $\hat{\boldsymbol{x}}$ (hybrid labeling) is algorithmic without requiring any look-up table. Thus, the proposed MLC scheme has a reasonable complexity despite the extremely large constellation size of 7.9×10^{28} for 24D VC. For a fair evaluation of the shaping gain, the same MLC scheme is applied to 256-QAM with 2 coded bits and 6 uncoded bits. An LDPC code with a fixed code rate is utilized for all signal formats to keep the same coded SE, while the detailed optimization of the code rate is explained in Section IV-B.

IV. Simulation

Based on the MLC scheme in Fig. 2, we perform Monte Carlo simulations for 256-QAM and 8/24-dimensional VCs at the same uncoded SE. An n-dimensional AWGN channel is considered for performance evaluation and expressed as

$$\boldsymbol{y} = \boldsymbol{x} + \boldsymbol{z} \tag{1}$$

where $\boldsymbol{z} = [z_1, z_2, \ldots, z_n]$ is a random vector with n independent real zero-mean Gaussian random variables having equal noise variance $\sigma_z^2 = \sigma_{z_1}^2 = \ldots = \sigma_{z_n}^2$. Given the total n-dimensional signal power of $\sigma_{\boldsymbol{x}}^2$ and noise variance of $\sigma_{\boldsymbol{z}}^2 = \sigma_{z_1}^2 + \sigma_{z_2}^2 + \ldots + \sigma_{z_n}^2 = n\sigma_z^2$, the overall SNR is defined as SNR$= \sigma_{\boldsymbol{x}}^2/\sigma_{\boldsymbol{z}}^2$.

Moreover, only a limited-length sequence can be applied to the experiment due to the memory limitation of the digital-to-analog converter (DAC). In our experiment, a single 64800-bit block with 2700 24D VC symbols is loaded to the DACs. To evaluate the effect of sequence length on VC performance, we first apply 10 blocks of VCs to the AWGN channel (referred to 10B in Fig. 3). As a reference to the experiment, we apply 1

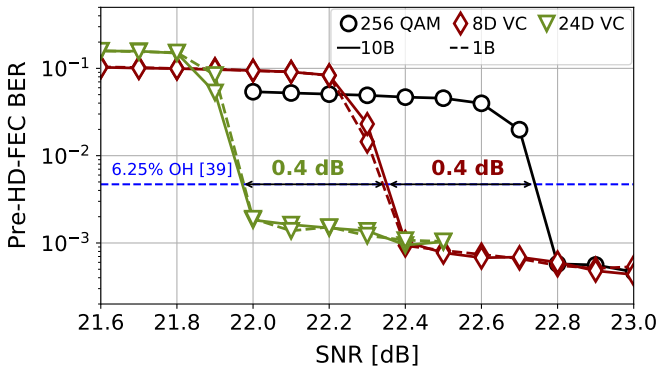

Fig. 3. Simulated BER after SD decoding (i.e., Pre-HD-FEC BER) vs SNR for 256-QAM, 8D and 24D VC for a fixed code rate R_c of 1/2. 10B: 10 blocks of VC signal; 1B: 1 blocks of VC signal.

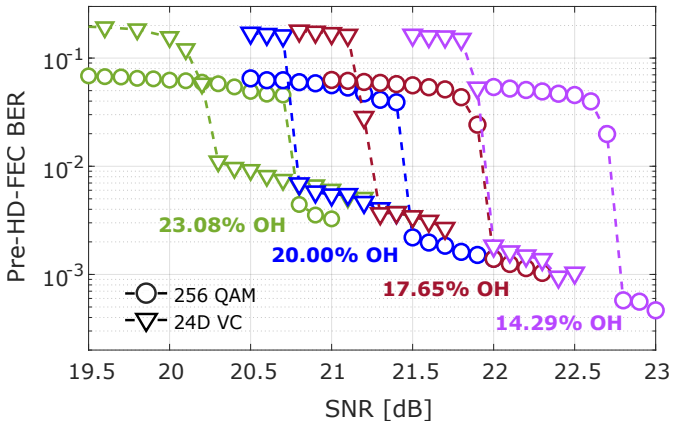

Fig. 4. Simulated pre-HD-FEC BER versus SNR for various code rates $R_c = \{1/2, 2/5, 1/3, 1/4\}$ with OHs of $\{14.29, 17.65, 20.00, 23.08\}\%$.

block of VCs to the AWGN channel (referred to 1B in Fig. 3) and repeat the simulation 10 times for a fair comparison. A DVB-S2 standard LDPC code is implemented in the MLC scheme. Assuming an outer HD code, we estimate the BER after LDPC decoding (i.e., pre-HD-FEC BER) to evaluate the system performance.

A. 8/24-Dimensional-VCs vs 256-QAM

We first fix the code rate to 1/2 and compare the shaping gain of these two VCs for the same coded SE. Figure 3 shows the pre-HD-FEC BER as a function of SNR for the three signal formats. Assuming an outer HD staircase code [39], the 8D and 24D VCs outperform 256-QAM by 0.4 and 0.8 dB at the BER threshold of 4.7×10^{-3}, respectively. As depicted in Fig. 1, the 24D VC has a 1D probability distribution that is closer to the Gaussian shape, providing twice as high gain as the 8D VC. Therefore, we disregard the 8D VC in the following, focusing on the 24D VC and 256-QAM.

In the proposed MLC scheme, a high error floor after the SD decoder is induced due to the uncoded bits. Therefore at a SNR $>$22.8 dB, the pre-HD-FEC BER for 256-QAM decreases to around 6×10^{-4} and from there decreases more slowly as the SNR increases further. The 8D and 24D VCs experience a similar error floor phenomenon starting from lower SNRs of 22.4 dB and 22.0 dB, respectively, due to the shaping gain. In contrast to the simulation with 10 blocks of different VCs, the case using 1 block of VC has similar performance and does not affect the shaping gain. This means that the limited sequence length induced by the DAC memory has negligible influence on the estimated VC performance.

B. Optimization of SD-FEC Overhead

We need to sweep the code rate to optimize the coded system performance at various SNRs. A set of code rates $R_c = \{1/2, 2/5, 1/3, 1/4\}$ with OHs of $\{14.29, 17.65, 20.00, 23.08\}\%$ are implemented to evaluate the system performance after SD decoding. Figure 4 illustrates the pre-HD-FEC BER versus SNR for the four code rates. As the SD-FEC OH increases from 14.29% to 23.08%, the shaping gain reduces from 0.8 dB to 0.5 dB. More importantly, a significantly higher error floor at a BER of around 1×10^{-2} is induced in the 23.08% OH case, requiring a higher HD-FEC OH to achieve error-free performance after the assumed HD decoding. The BER error floor generated by the uncoded bits leads to a significant penalty due to the increased HD-FEC OH, especially for the SD-FEC OH of 20.00% and 23.08%. Therefore, the SD-FEC OH should be independently optimized for each system with a given SNR to obtain minimum pre-HD-FEC BER and coded OH (i.e., SD- and HD-FEC OH).

V. Experimental Setup

The experimental setup is shown in Fig. 5(a). We use three test-band channels and amplified spontaneous emission (ASE) noise-based loading channels. The optical carrier generated by an external cavity laser (ECL) of $<$100 kHz linewidth is divided into four arms by three 3-dB couplers for each polarization in the center and side channels of the testband. During the measurements, the wavelength of the ECL is swept over the C-band in steps of one channel (i.e., 5.2 GHz). We employ 5.0 Gbaud 256-QAM and 24D VC pulse-shaped with a 1% roll-off root-raised-cosine filter. The relatively low symbol rate is used to eliminate the transceiver impairments. The 24D constellation points are modulated across both quadratures, both polarizations, and six time slots. A static digital pre-emphasis filter and an arcsine function/memory-5 look-up-table based pre-distortion [40], [41] are used to mitigate the linear and nonlinear transmitter impairments, respectively. In the center channel, the electrical signals generated by four 60 GS/s DACs with 7.0 effective number of bits at 5 GHz are electrically amplified and fed to two I/Q modulators. Two variable optical attenuators (VOA) are used to balance the optical power of each polarization before the polarization beam combiner. To generate the side channels, we first digitally shift two independent signals by $\pm$5.2 GHz and combine them to form a digital double-sideband signal, which is loaded into the DACs to generate the side channels using the same modulator. The test-band channels are then combined and amplified by a booster before adjusting the launch power with a VOA. Two C-band erbium-doped fiber amplifiers (EDFAs) and wavelength-selective switches (WSSs) are used to generate

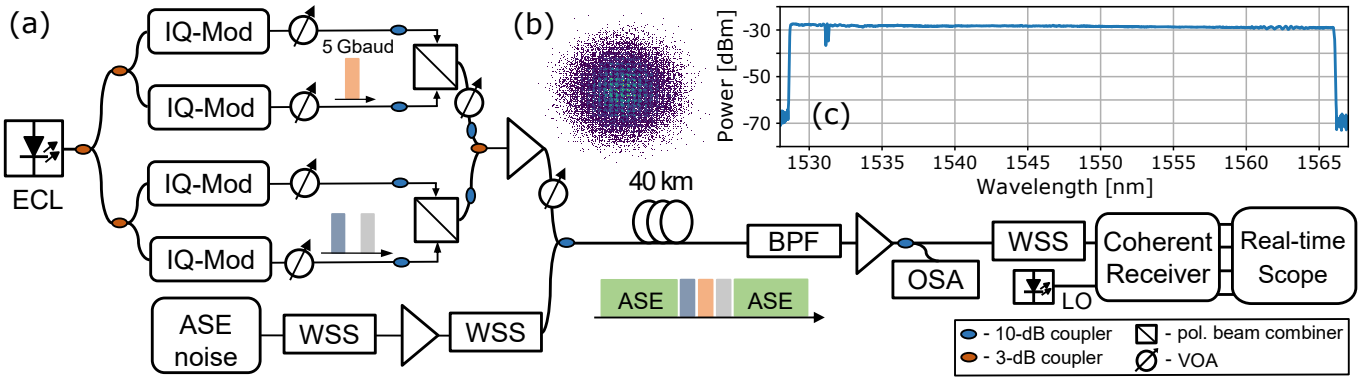

Fig. 5. (a) Experimental setup for C-band transmission of 40 km fiber, (b) Received 24D Voronoi constellation, (c) C-band spectrum including the test and loading channels. Here the test band is centered at 1531.45 nm.

the loading channels and suppress the ASE noise for the test band. Importantly, the second EDFA in the loading-band generation is set to the maximum output power of 30 dBm to provide a high launch power. The VOA and WSS equalize the power spectral density for the signal and ASE channel. The test band and loading band are then combined in a 10-dB coupler and transmitted over a 40 km single-mode fiber. The C-band spectrum including test-band channels centered at 1531.45 nm and ASE-based loading-band channels is shown in Fig. 5(c).

At the receiver, a band-pass filter (BPF), an EDFA, and a WSS are employed to amplify and filter the center channel, which is the only measured channel out of the three test-band channels. The coherently detected signal is sampled by an 80 GS/s oscilloscope before applying a pilot-based offline DSP [42], including static chromatic dispersion compensation, downsampling and matched filtering, frequency offset estimation (FOE), synchronization, dynamic equalization and carrier phase estimation (CPE). A pilot sequence located at the beginning of the frame and periodically inserted phase pilots are used for FOE/equalization and CPE, respectively. A frame length of 16896, a pilot sequence length of 512, and an insertion ratio of 1/128 lead to an optimized digital pilot OH of 3.93%. The post-processed 24D VC is depicted in Fig. 5(b). Importantly, the 24D VC needs to be shifted with its original small mean for demodulation. Finally, we perform multilevel decoding before estimating the pre-HD-FEC BER. To optimize the SD-FEC OH, we set the total launch power to 18 dBm and estimate the SNR after 40 km transmission. As shown in Fig. 4, a measured SNR of 23 dB for 256-QAM requires applying the 14.29% SD-FEC OH to maximize the system performance. Therefore, a fixed code rate of 1/2 is implemented for 256-QAM and 24D VC in the C-band transmission measurements.

VI. Experimental Results

For a fair comparison, we transmit the 256-QAM and 24D VC with a fixed code rate of 1/2 over the 40 km SMF. We first estimate the system performance with varying launch powers to investigate the shaping gain and obtain the optimum launch power for C-band transmission. Then we apply the same optimized launch power to all the wavelengths and evaluate the C-band transmission performance.

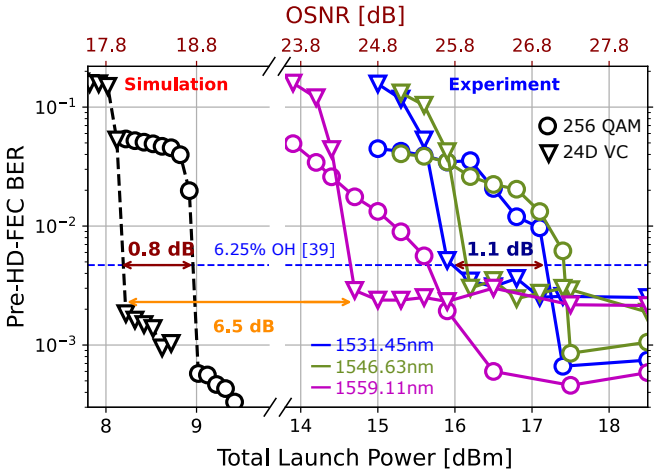

Fig. 6. Pre-HD-FEC BER versus total launch power at the wavelength of 1531.45 nm, 1546.63 nm, and 1559.11 nm.

A. Pre-HD-FEC BER vs Launch Power

Figure 6 shows the estimated pre-HD-FEC BER for 256-QAM and 24D VC versus launch power/OSNR for the center channel at 1531.45 nm, 1546.63 nm, and 1559.11 nm. For a given launch power, the single-channel OSNR in dB is

$$\mathrm{OSNR} = 58 + (P_{\mathrm{tot}} - \Delta P) - L_{\mathrm{fiber}} - L_{\mathrm{BPF}} - NF \quad (2)$$

$$\Delta P = 10\log_{10}(N_{\mathrm{ch}}) \quad (3)$$

where P_{tot} is the total launch power in decibel-milliwatt (dBm), ΔP is the power difference in decibels between one channel and the whole C-band signal, N_{ch} is the number of wavelength channels in the C-band (i.e., $N_{\mathrm{ch}} = 854$), L_{fiber} is the 40-km fiber loss of around 8.4 dB, L_{BPF} is the receiver BPF loss of 5 dB, and NF is the noise figure of 5.5 dB. The simulated performance for the applied signal formats is included for comparison and the OSNR of the simulated signal in dB is

$$\mathrm{OSNR}_{\mathrm{sim}} = \mathrm{SNR}_{\mathrm{sim}} + 10\log_{10}\left(\frac{B_{\mathrm{sig}}}{B_{\mathrm{o}}}\right) \quad (4)$$

where $\mathrm{SNR}_{\mathrm{sim}}$ is the simulated SNR, B_{sig} is the applied optical signal bandwidth of 5 GHz/0.04 nm, and B_{o} is the reference noise bandwidth of 0.1 nm. Assuming an outer HD staircase

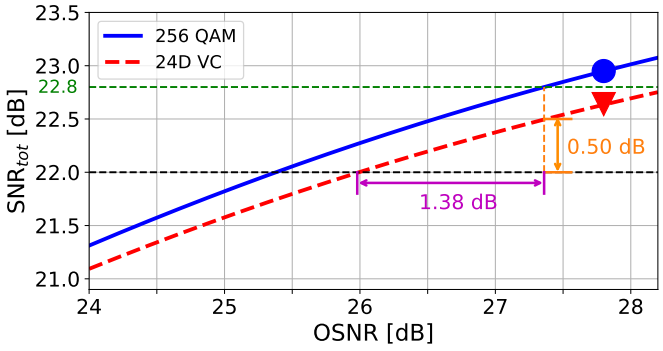

Fig. 7. Simulated SNR versus OSNR for 256-QAM and 24D VC. The marker indicates the estimated experimental SNR at OSNR=27.8 dB for the center wavelength of 1546.63 nm.

TABLE I
ESTIMATED TRANSCEIVER SNR

Modulation Formats	Transceiver SNR / dB		
	1531.45 nm	1546.63 nm	1559.11 nm
256-QAM	24.76	24.67	25.27
24D VC	24.45	24.25	24.79

code with 6.25% OH and a BER threshold of 4.7×10^{-3} [39], the 24D VC outperforms 256-QAM by around 1.1 dB in terms of OSNR for all three wavelengths, which is higher than the simulated SNR gain of 0.8 dB. This is because the transmitter's electrical noise is dominant, meaning that the SNR gain will correspond to a higher OSNR gain. A penalty of around 6.5 and 7.7 dB is induced for the 24D VC at the wavelength of 1559.11 nm and 1531.45/1546.63 nm, respectively, due to the wavelength-dependent transceiver and channel impairments. Considering the implementation penalty difference compared with 256-QAM, the 24D VC still achieves >1 dB shaping gain for all three measured wavelengths. Clearly, we observe an error floor similar to the simulated results shown in Fig. 4. By sweeping the input power to the fiber and comparing the pre-HD-FEC BER, we find that the optimum launch power is around 20 dBm, which is used for all the wavelengths in the C-band transmission measurements.

To further quantify the experimental penalty for VCs at different wavelengths, we estimated the SNR for all the modulation formats at the launch power of 18 dBm, which corresponds to the OSNR of 27.8 dB. The measured SNR for 256-QAM is 23.01 dB, 22.95 dB, and 23.34 dB at the wavelengths of 1531.45nm, 1546.63 nm, and 1559.11 nm, while the corresponding SNR for 24D VC is 22.80 dB, 22.66 dB, and 23.03 dB. We simulate the total SNR in a system including transceiver noise and ASE noise to find the relationship between OSNR improvement and SNR gain

$$\mathrm{SNR_{tot}} = \frac{\sigma_{\mathrm{sig}}^2}{\sigma_{\mathrm{TRx}}^2 + \sigma_{\mathrm{ASE}}^2} = \frac{1}{\frac{1}{\mathrm{SNR_{TRx}}} + \frac{1}{\mathrm{OSNR}}} \tag{5}$$

where σ_{sig}^2 is the signal power, σ_{TRx}^2 is the transceiver noise variance, and σ_{ASE}^2 is the ASE noise variance. Following Eq. 5 and the experimentally measured SNR at OSNR=27.8 dB, the calculated transceiver SNR ($\mathrm{SNR_{TRx}}$) is given in Table I. An average penalty of 0.40 dB is induced by the transceiver impairments, resulting in a fundamental shaping gain of 0.40 dB. As shown in Fig. 7, the blue solid line is the simulated total SNR for 256QAM at the wavelength of 1546.63 nm, which matches the measured SNR at OSNR of 27.8 dB, while the red dashed line is the estimated SNR for 24D VC. The 0.50 dB gain corresponds to an OSNR improvement of 1.38 dB, which is similar to the experimental improvement in OSNR. In this regime, both transceiver noise and ASE noise have a significant contribution to the total SNR. Therefore, a large OSNR change only results in a small variation of the overall SNR.

B. C-band Transmission Performance

Sweeping the center wavelength of the test band from 1530 to 1565.5 nm, the measured pre-HD-FEC BER for 24D VC for 854 wavelength channels after 40 km SMF is shown in Fig. 8. We achieve error-free transmission for all 854 wavelengths in the C-band as the BERs are below the HD-FEC threshold. Accounting for the 14.29% SD-FEC OH, 6.25% HD-FEC OH, 4.00% OH for interchannel guard bands, and 3.93% digital pilot OH, we achieve an overall SE of 12.2 bit/s/Hz and a throughput of 54.2 Tb/s in the C-band spectrum of 4.44 THz. The guard bands and pilot OH can be further reduced by using an ultra-narrow-linewidth (e.g., 100 Hz) coherent laser, joint phase recovery [43] and joint equalization [44] in a comb-based superchannel. Moreover, since only 24 of 96 bits are encoded for the 24D VC, inducing a high pre-HD-FEC BER after SD decoding, the 6.25% HD-FEC OH

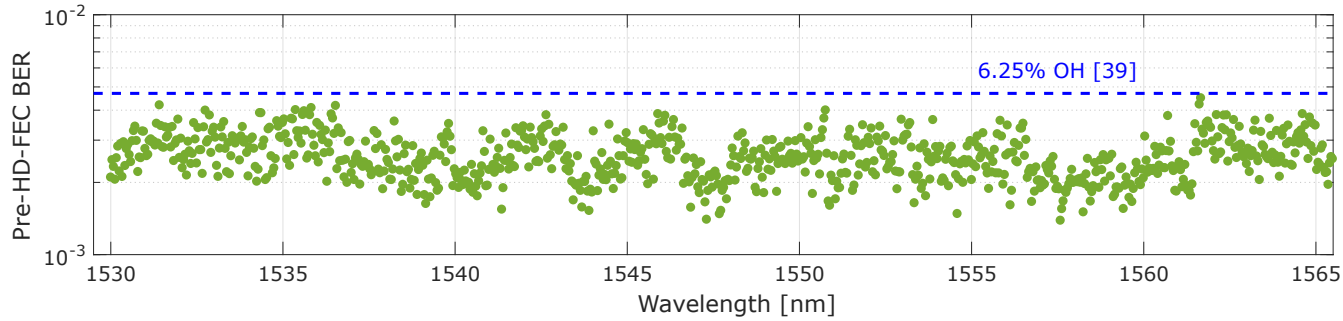

Fig. 8. Measured performance after 40 km SMF. Pre-HD-FEC BER for 854 24D VC channels covering the whole C-band from 1530 nm to 1565.5 nm.

can be significantly reduced by encoding more bits in the MLC schemes for error correction. The relatively low symbol rate is used to minimize impairments from our electronic and electro-optic components. However, the scheme is fully compatible with high symbol-rate transmission using state-of-the-art transceivers.

VII. Conclusion

We demonstrated the largest cardinality constellation ever of 7.9×10^{28} symbols for a fully loaded C-band system with 854×5.0 Gbaud 24D VC, achieving a high SE of 12.2 bit/s/Hz and an overall throughput of 54.2 Tb/s after 40 km transmission. This is the first experimental demonstration of MD modulation formats achieving a significant shaping gain over QAM after SD decoding at >12 bit/s/Hz SE over the whole C-band, showing the potential of applying MD VCs in high-SE high-throughput systems. It may be particularly beneficial in space-division multiplexing systems with more available dimensions. For example, the 24D VC could be applied to dual-polarization coherent transmission over two wavelengths and all three cores in a 3-core space-division multiplexing fiber to perform joint encoding and maximize the system throughput.

Acknowledgments

This work was supported by Knut and Alice Wallenberg Foundation (KAW 2018-0090) and the Swedish Research Council projects 2019-04078 and 2021-03709.

References

[1] P. W. Berenguer, M. Nölle, L. Molle, T. Raman, A. Napoli, C. Schubert, and J. K. Fischer, "Nonlinear digital pre-distortion of transmitter components," *J. Lightw. Technol.*, vol. 34, no. 8, pp. 1739–1745, 2016.

[2] D. S. Millar, R. Maher, D. Lavery, T. Koike-Akino, M. Pajovic, A. Alvarado, M. Paskov, K. Kojima, K. Parsons, B. C. Thomsen, S. J. Savory, and P. Bayvel, "Design of a 1 Tb/s superchannel coherent receiver," *J. Lightw. Technol.*, vol. 34, no. 6, pp. 1453–1463, 2016.

[3] H. Sun, M. Torbatian, M. Karimi, R. Maher, S. Thomson, M. Tehrani, Y. Gao, A. Kumpera, G. Soliman, A. Kakkar, M. Osman, Z. A. El-Sahn, C. Doggart, W. Hou, S. Sutarwala, Y. Wu, M. R. Chitgarha, V. Lal, H.-S. Tsai, S. Corzine, J. Zhang, J. Osenbach, S. Buggaveeti, Z. Morbi, M. I. Olmedo, I. Leung, X. Xu, P. Samra, V. Dominic, S. Sanders, M. Ziari, A. Napoli, B. Spinnler, K.-T. Wu, and P. Kandappan, "800G DSP ASIC design using probabilistic shaping and digital sub-carrier multiplexing," *J. Lightw. Technol.*, vol. 38, no. 17, pp. 4744–4756, 2020.

[4] "Infinera 800 G," 2020. [Online]. Available: https://www.infinera.com/press-release/infinera-breaks-industry-record-with-800g-transmission-over-950-kilometers-in-a-live-network-trial.

[5] "Huawei 800 G," 2020. [Online]. Available: https://www.huawei.com/en/news/2020/2/800g-tunable-ultra-high-speed-optical-module.

[6] F. Pittalà, G. Böcherer, P. Schulte, M. Schaedler, S. Calabrò, B. Zheng, C. Xie, and M. Kuschnerov, "72.64 Tb/s DWDM transmission over 100 km G.654D fiber using super C-band erbium-doped fiber amplification," in *Proc. Opt. Fiber Commun. Conf.*, 2022, Paper W3C.4.

[7] Y. Yu, L. Jin, Y. Lu, Y. Huang, and L. Li, "400×377.6 Gb/s C+L band seamless transmission over 200 km with raman amplifier using PDM-256QAM," in *Proc. Eur. Conf. Opt. Commun.*, 2018, Paper Th2.49.

[8] M. Ionescu, L. Galdino, A. Edwards, J. James, W. Pelouch, E. Sillekens, D. Semrau, D. Lavery, R. I. Killey, S. Barnes, P. Bayvel, and S. Desbruslais, "91 nm C+L hybrid distributed Raman-Erbium-Doped fibre amplifier for high capacity subsea transmission," in *Proc. Eur. Conf. Opt. Commun.*, 2018, Paper Mo4G.2.

[9] X. Zhao, S. Escobar-Landero, D. L. Gac, A. Lorences-Riesgo, T. Viret-Denaix, Q. Guo, L. Gan, S. Li, S. Cao, X. Xiao, N. E. Dahdah, A. Gallet, S. Yu, H. Hafermann, L. Godard, R. Brenot, Y. Frignac, and G. Charlet, "200.5 Tb/s transmission with S+C+L amplification covering 150 nm bandwidth over 2×100 km PSCF spans," in *Proc. Eur. Conf. Opt. Commun.*, 2022, Paper Th3C.4.

[10] B. J. Puttnam, R. S. Luís, G. Rademacher, M. Mendez-Astudillio, Y. Awaji, and H. Furukawa, "S-, C- and L-band transmission over a 157 nm bandwidth using doped fiber and distributed Raman amplification," *Opt. Express*, vol. 30, no. 6, pp. 10 011–10 018, 2022.

[11] M. Mazur, J. Schröder, A. Lorences-Riesgo, T. Yoshida, M. Karlsson, and P. A. Andrekson, "12 b/s/Hz spectral efficiency over the C-band based on comb-based superchannels," *J. Lightw. Technol.*, vol. 37, no. 2, pp. 411–417, 2019.

[12] F. Pittalà, R.-P. Braun, G. Böcherer, P. Schulte, M. Schaedler, S. Bettelli, S. Calabrò, M. Kuschnerov, A. Gladisch, F.-J. Westphal, C. Xie, R. Chen, Q. Wang, and B. Zheng, "1.71 Tb/s single-channel and 56.51 Tb/s DWDM transmission over 96.5 km field-deployed SSMF," *IEEE Photon. Technol. Lett.*, vol. 34, no. 3, pp. 157–160, 2022.

[13] D. Qian, M.-F. Huang, E. Ip, Y.-K. Huang, Y. Shao, J. Hu, and T. Wang, "101.7-Tb/s (370×294-Gb/s) PDM-128QAM-OFDM transmission over 3×55-km SSMF using pilot-based phase noise mitigation," in *Proc. Opt. Fiber Commun. Conf.*, 2011, Paper PDPB5.

[14] G. Forney, R. Gallager, G. Lang, F. Longstaff, and S. Qureshi, "Efficient modulation for band-limited channels," *IEEE J. Sel. Areas Commun.*, vol. 2, no. 5, pp. 632–647, 1984.

[15] P. Schulte and G. Böcherer, "Constant composition distribution matching," *IEEE Trans. Inf. Theory*, vol. 62, no. 1, pp. 430–434, 2016.

[16] E. Sillekens, G. Liga, D. Lavery, P. Bayvel, and R. I. Killey, "High-cardinality geometrical constellation shaping for the nonlinear fibre channel," *J. Lightw. Technol.*, vol. 40, no. 19, pp. 6374–6387, 2022.

[17] R. T. Jones, M. P. Yankov, and D. Zibar, "End-to-end learning for GMI optimized geometric constellation shape," in *Proc. Eur. Conf. Opt. Commun.*, 2019, Paper W.1.B.

[18] R. Dar, M. Feder, A. Mecozzi, and M. Shtaif, "On shaping gain in the nonlinear fiber-optic channel," in *Proc. IEEE Int. Symp. Inf. Theory*, 2014, pp. 2794–2798.

[19] B. Chen, C. Okonkwo, H. Hafermann, and A. Alvarado, "Polarization-ring-switching for nonlinearity-tolerant geometrically shaped four-dimensional formats maximizing generalized mutual information," *J. Lightw. Technol.*, vol. 37, no. 14, pp. 3579–3591, 2019.

[20] K. Kojima, T. Yoshida, T. Koike-Akino, D. S. Millar, K. Parsons, M. Pajovic, and V. Arlunno, "Nonlinearity-tolerant four-dimensional 2A8PSK family for 5–7 bits/symbol spectral efficiency," *J. Lightw. Technol.*, vol. 35, no. 8, pp. 1383–1391, 2017.

[21] G. Ungerboeck, "Channel coding with multilevel/phase signals," *IEEE Trans. Inf. Theory*, vol. 28, no. 1, pp. 55–67, 1982.

[22] D. S. Millar, T. Koike-Akino, S. Ö. Arık, K. Kojima, K. Parsons, T. Yoshida, and T. Sugihara, "High-dimensional modulation for coherent optical communications systems," *Opt. Express*, vol. 22, no. 7, pp. 8798–8812, 2014.

[23] E. Agrell and M. Karlsson, "Power-efficient modulation formats in coherent transmission systems," *J. Lightw. Technol.*, vol. 27, no. 22, pp. 5115–5126, 2009.

[24] T. A. Eriksson, P. Johannisson, M. Sjödin, E. Agrell, P. A. Andrekson, and M. Karlsson, "Frequency and polarization switched QPSK," in *Proc. Eur. Conf. Opt. Commun.*, 2013, Paper Th.2.D.4.

[25] T. A. Eriksson, P. Johannisson, E. Agrell, P. A. Andrekson, and M. Karlsson, "Biorthogonal modulation in 8 dimensions experimentally implemented as 2PPM-PS-QPSK," in *Proc. Opt. Fiber Commun. Conf.*, 2014, Paper W1A.5.

[26] J. Conway and N. Sloane, "A fast encoding method for lattice codes and quantizers," *IEEE Trans. Inf. Theory*, vol. 29, no. 6, pp. 820–824, 1983.

[27] G. Forney, "Multidimensional constellations. II. Voronoi constellations," *IEEE J. Sel. Areas Commun.*, vol. 7, no. 6, pp. 941–958, 1989.

[28] A. Mirani, K. Vijayan, S. Li, Z. He, J. Schröder, P. Andrekson, E. Agrell, and M. Karlsson, "Comparison of physical realizations of multidimensional Voronoi constellations in single mode fibers," in *Proc. Eur. Conf. Opt. Commun.*, 2022, Paper We5.39.

[29] A. Mirani, K. Vijayan, S. Li, Z. He, E. Agrell, J. Schröder, P. Andrekson, and M. Karlsson, "Physical realizations of multidimensional Voronoi constellations in optical communication systems," *J. Lightw. Technol.*, vol. 41, no. 17, pp. 5557–5563, 2023.

[30] J. H. Conway and N. J. A. Sloane, "Fast quantizing and decoding algorithms for lattice quantizers and codes," *IEEE Trans. Inf. Theory*, vol. IT-28, no. 2, pp. 227–232, 1982.

[31] B. M. Kurkoski, "Encoding and indexing of lattice codes," *IEEE Trans. Inf. Theory*, vol. 64, no. 9, pp. 6320–6332, 2018.
[32] R.-J. Essiambre, R. Ryf, S. v. der Heide, J. I. Bonetti, H. Huang, M. Kodialam, F. J. García-Gómez, E. C. Burrows, J. C. Alvarado-Zacarias, R. Amezcua-Correa, X. Chen, N. K. Fontaine, and H. Chen, "First transmission of a 12D format across three coupled spatial modes of a 3-core coupled-core fiber at 4 bits/s/Hz," in *Proc. Opt. Fiber Commun. Conf.*, 2020, paper Th3H.4.
[33] S. Li, A. Mirani, M. Karlsson, and E. Agrell, "Low-complexity Voronoi shaping for the Gaussian channel," *IEEE Trans. Commun.*, vol. 70, no. 2, pp. 865–873, 2022.
[34] ——, "Power-efficient Voronoi constellations for fiber-optic communication systems," *J. Lightw. Technol.*, vol. 41, no. 5, pp. 1298–1308, 2023.
[35] ——, "Coded modulation schemes for Voronoi constellations," *arxiv:2308.00407*, pp. 1–13, 2023.
[36] A. Mirani, E. Agrell, and M. Karlsson, "Low-complexity geometric shaping," *J. Lightw. Technol.*, vol. 39, no. 2, pp. 363–371, 2021.
[37] J. Conway and N. Sloane, "A fast encoding method for lattice codes and quantizers," *IEEE Trans. Inf. Theory*, vol. 29, no. 6, pp. 820–824, 1983.
[38] A. Alvarado, T. Fehenberger, B. Chen, and F. M. J. Willems, "Achievable information rates for fiber optics: Applications and computations," *J. Lightw. Technol.*, vol. 36, no. 2, pp. 424–439, 2018.
[39] L. M. Zhang and F. R. Kschischang, "Staircase codes with 6% to 33% overhead," *J. Lightw. Technol.*, vol. 32, no. 10, pp. 1999–2002, 2014.
[40] Z. He, K. Vijayan, M. Mazur, M. Karlsson, and J. Schröder, "Look-up table based pre-distortion for transmitters employing high-spectral-efficiency modulation formats," in *Proc. Eur. Conf. Opt. Commun.*, 2020, Paper Tu1D.6.
[41] Z. He, J. Song, K. Vijayan, C. Häger, A. G. i. Amat, H. Wymeersch, P. A. Andrekson, M. Karlsson, and J. Schröder, "Periodicity-enabled size reduction of symbol based predistortion for high-order QAM," *J. Lightw. Technol.*, vol. 40, no. 18, pp. 6168–6178, 2022.
[42] M. Mazur, J. Schröder, A. Lorences-Riesgo, T. Yoshida, M. Karlsson, and P. A. Andrekson, "Overhead-optimization of pilot-based digital signal processing for flexible high spectral efficiency transmission," *Opt. Express*, vol. 27, no. 17, pp. 24 654–24 669, 2019.
[43] L. Lundberg, M. Mazur, A. Mirani, B. Foo, J. Schröder, V. Torres-Company, M. Karlsson, and P. A. Andrekson, "Phase-coherent lightwave communications with frequency combs," *Nat. Commun.*, vol. 11, no. 201, 2020.
[44] Z. He, K. Vijayan, A. Mirani, M. Karlsson, and J. Schröder, "Inter-channel interference cancellation for long-haul superchannel system," *J. Lightw. Technol.*, pp. 1–9, 2023.